Periodic Trends in Electrode−Chemisorbate Bonding: Benzonitrile on Platinum-Group and Other Noble Metals As Probed by Surface-Enhanced Raman Spectroscopy Combined with Density Functional Theory

Melissa F. Mrozek, Sally A. Wasileski, and Michael J. Weaver*

Contribution from the Department of Chemistry, Purdue University, West Lafayette, Indiana 47907-1393

Received January 4, 2001

Abstract: Detailed intramolecular vibrational spectra obtained by means of surface-enhanced Raman scattering (SERS) for benzonitrile adsorbed on seven electrode surfaces—four Pt-group metals (platinum, palladium, rhodium, and iridium) and the Group IB metals (copper, silver, and gold)—are reported with the aim of exploring the metal-dependent nature of surface−chemisorbate interactions. The Pt-group surfaces were prepared as ultrathin electrodeposited films on gold, enabling the SERS activity inherent to the substrate to be imparted to the overlayer material. Benzonitrile was selected as a "model" organic adsorbate since it displays a rich array of coupled aromatic ring as well as substituent modes which collectively can provide insight into the various molecular perturbations induced by surface coordination via the nitrile substituent. The experimental spectra are compared with ab initio calculations of vibrational frequencies, bond geometries, and charge distributions obtained by means of Density Functional Theory (DFT), which yields valuable insight into the underlying structural reasons for the sensitivity of the experimental coordination-induced frequency shifts to the nature of the intramolecular mode and the metal surface. The DFT results also form an invaluable aid in making SER spectral assignments, along with providing detailed information on the coupled atomic displacements involved in each vibrational mode. Benzonitrile surface coordination was modeled in the DFT calculations by binding the nitrile group to metal atoms and small metal clusters. While the majority of the aromatic-ring SER frequencies are altered only slightly ($\lesssim$5 cm^{-1}) upon surface coordination, several modes (especially ν_1, ν_{6a}) are blue-shifted substantially (by up to 50 cm^{-1}). These shifts were identified by DFT as arising from mode coupling to the nitrile substituent, especially involving the C−CN bond that is compressed upon nitrile coordination, associated with metal−adsorbate back-donation. The small (<5 cm^{-1}) red-shifts seen for ring vibrations not involving coupled substituent motion apparently arise from increased antibonding aromatic electron density. The metal-dependent frequency shifts seen for these coupled aromatic vibrations as well as for the more localized C−N nitrile stretching mode are consistent with increased back-donation anticipated in the sequence $d^{10} < d^9 < d^8$ within a given Periodic row. Overall, the findings provide a benchmark illustration of the virtues of DFT in interpreting complex vibrational spectra for larger polyatomic adsorbates.

Introduction

Understanding how the nature of chemisorbate binding depends on the chemical nature of the metal surface constitutes an issue of major fundamental significance in electrochemistry as well as in ultrahigh vacuum (UHV)-based surface science. For the latter type of interface, experimental information regarding metal−chemisorbate interactions is attainable in several ways, including temperature-dependent desorption along with electronic and vibrational spectroscopies. For in situ electrochemical interfaces, however, the breadth of available molecular-level probes is considerably narrower. Although infrared reflection-absorption spectroscopy (IRAS) has found extensive application at electrochemical (EC) as well as metal−UHV interfaces, the limitations set by sensitivity, selection rules, and solution-phase interferences place restrictions on the type of vibrational modes (and hence the range of adsorbate molecules) suitable for characterization by EC-IRAS. The other type of vibrational technique commonly applied to electrochemical interfaces, surface-enhanced Raman spectroscopy (SERS), offers typically higher sensitivity, more liberal selection rules, and a wider effective wavenumber range. As a consequence, SERS often yields much richer vibrational spectra than IRAS, including the ability to detect surface−adsorbate and other low-frequency vibrations, and the common appearance of most (if not all) normal modes of polyatomic molecules. Indeed, these attributes of SERS are in some respects comparable to those of electron energy-loss spectroscopy (EELS), although the latter suffers from poorer wavenumber resolution and is only applicable to UHV-based interfaces. However, the usual need to employ coinage-metal substrates would appear to limit severely the types of interfaces amenable to characterization by SERS.

Mindful of the unique virtues of SERS for the detailed vibrational characterization of metal−ambient interfaces, we have long been interested in expanding its applicability to surface materials beyond the coinage metals.[1−4] Our primary

* Address correspondence to this author. E-mail: mweaver@purdue.edu.

(1) For a recent overview, see: Weaver, M. J.; Zou, S.; Chan, H. Y. H. *Anal. Chem.* **2000**, *72*, 38A.

(2) (a) Leung, L.-W. H.; Weaver, M. J. *J. Am. Chem. Soc.* **1987**, *109*, 5113. (b) Leung, L.-W. H.; Weaver, M. J. *Langmuir* **1988**, *4*, 1076.

10.1021/ja010049k CCC: $20.00
Published on Web 12/01/2001

tactic involves electrodepositing the material of interest as an ultrathin (nanoscale) film onto gold.[1] This exploits the chemical (and electrochemical) inertness as well as excellent SERS properties of gold, along with the demonstrated ability to impart substantial Raman enhancement to species bound to the outer surface of (and also within) the overlayer film. The strategy has been utilized in particular to explore chemisorption on platinum-group metal surfaces in elevated-temperature gaseous as well as in electrochemical environments, prompted by their catalytic importance, although a variety of other interfaces have also been scrutinized in this manner, including oxides and semiconductors.[3] The range of adsorbates examined at Pt-group electrodes with our "overlayer-SERS" strategy was limited originally by the presence of residual exposed gold sites, which can yield spectral and electrochemical interferences. More recently, however, we have devised modified electrodeposition procedures that yield ultrathin (3−5 monolayer) Pt-group metal overlayers displaying optimal SERS properties that are essentially pinhole-free, and thereby devoid of substrate interferences.[6] While thicker films yield progressively weaker SERS signals, a significant and eventually dominant contribution to the Raman enhancement has been shown to emanate from the transition-metal overlayer itself.[7] These developments therefore enable us to acquire vibrational spectra for a much wider range of adsorbates at transition-metal electrochemical interfaces, including species that bind also to gold electrodes. Indeed, we have recently utilized this tactic to obtain potential-dependent vibrational spectra at Pt-group electrodes for a variety of chemisorbates, including halides,[8a] pseudohalides,[8b] sulfur,[8a] oxides,[9] alkenes,[10] and aromatic molecules.[11]

As a consequence, SERS can now be harnessed to explore in broad-based fashion the sensitivity of chemisorbate vibrational properties to the electrode material. We recently examined periodic trends in monatomic chemisorbate bonding on four Group VIII metals (Pt, Pd, Ir, and Rh) along with the three Group IB metals (Cu, Ag, Au) by monitoring the SERS surface−adsorbate stretching mode as a function of electrode potential.[8] The rich vibrational spectra attainable by SERS for aromatic chemisorbates furnishes a more complex, yet chemically important, class of systems with which to explore such periodic trends. We have chosen benzonitrile (C_6H_5CN) for initial detailed examination along these lines. Earlier SERS studies on gold[12] and palladium[11] have shown that benzonitrile binds to these metals via the nitrile substituent. While some Raman bands associated with the pendant aromatic ring are virtually unaltered in frequency (and band shape) from those for uncoordinated benzonitrile, other ring modes (along with the C−N vibration for the surface-attached nitrile group) are shifted to an extent that is sensitive to the electrode material.

The present report provides a detailed SERS-based analysis of the metal-dependent vibrational properties of benzonitrile chemisorbed on seven electrode surfaces, specifically for four Pt-group metals (Pt, Pd, Ir, and Rh) along with the three coinage metals (Cu, Ag, and Au). We have also undertaken ab initio calculations of the benzonitrile vibrational frequencies by means of Density Functional Theory (DFT), with the objective of elucidating the underlying structural reasons for the sensitivity of the chemisorption-induced frequency shifts to the nature of the intramolecular mode and the metal surface. The findings provide a benchmark illustration of the value of DFT for aiding the interpretation of the rich vibrational spectra attainable for larger polyatomic adsorbates by using SERS, as well as furnishing detailed insight into the relation between the vibrational properties and the nature of electrode−chemisorbate bonding.

Experimental and Computational Procedures

The experimental arrangement used for SERS is detailed in ref 15. The Raman excitation was from a Spectra Physics Stabilite model 2017 Kr^+ laser operated at 647.1 nm, with ca. 30 mW incident power focused to a 1 mm spot on the electrode surface. Scattered light was collected with a SPEX Triplemate spectrometer equipped with a Photometrics PM 512 CCD detector. The gold, silver, and copper electrodes were of rotating-disk construction, consisting of 2−4 mm diameter disks sheathed in Teflon, polished with 1.0 and 0.3 μm alumina and rinsed before use. Electrochemical roughening of the gold surface to yield optimal SERS activity consisted of successive oxidation−reduction cycles in 0.1 M KCl as outlined in ref 16. Similar electrochemical roughening procedures were performed for silver and copper electrodes as described in refs 17 and 18, respectively. Transition-metal SERS-active surfaces were prepared by constant-current electrodeposition onto a roughened gold electrode following the procedures outlined in ref 6. Typically, 3−5 monolayers were deposited, using either an acidic medium, 0.1 M $HClO_4$ (for Pd and Rh), or a phosphate buffer solution, 0.7 M Na_2HPO_4 (for Pt and Ir).[6] Electrolytes were prepared with ultrapure water from a Millipore MilliQ system. All measurements were made at room temperature (23 ± 1 °C), and all electrode potentials are reported versus a saturated calomel electrode (SCE).

Bis(benzonitrile)dichloroplatinum was synthesized as described in ref 19. $PtCl_2$ (Aldrich) was dissolved in a minimum volume of benzonitrile at 100 °C and stirred for 1 day. The yellow precipitate of *cis*-$PtCl_2(C_6H_5CN)_2$ was obtained after the solution was cooled and filtered. More product could be obtained by diluting the filtrate with light petroleum (bp 40−60 °C). The product was recrystallized in benzene, washed with water and ethanol, and dried in vacuo.

The DFT calculations reported here model chemisorbed benzonitrile by binding the lead-in nitrogen to three types of atop metal sites. The chief approach used involves only a single metal atom. While clearly not a quantitative model of a metal surface (!), as noted below this

(3) (a) Desilvestro, J.; Corrigan, D. A.; Weaver, M. J. *J. Phys. Chem.* **1986**, *90*, 6408. (b) Zou, S.; Weaver, M. J. *J. Phys. Chem. B* **1999**, *103*, 2323.

(4) (a) Leung, L.-W. H.; Weaver, M. J. *J. Electroanal. Chem.* **1987**, *217*, 367. (b) Leung, L.-W. H.; Gosztola, D.; Weaver, M. J. *Langmuir* **1987**, *3*, 45.

(5) For example: (a) Williams, C. T.; Takoudis, C. G.; Weaver, M. J. *J. Phys. Chem. B* **1998**, *102*, 406. (b) Tolia, A.; Williams, C. T.; Takoudis, C. G.; Weaver, M. J. *J. Phys. Chem.* **1995**, *99*, 4599.

(6) (a) Zou, S.; Weaver, M. J. *Anal. Chem.* **1998**, *70*, 2387. (b) Zou, S.; Gómez, R.; Weaver, M. J. *Langmuir* **1997**, *13*, 6713. (c) Mrozek, M. F.; Xie, Y.; Weaver, M. J. *Anal. Chem.* **2001**, *74*, 5953.

(7) Zou, S.; Weaver, M. J.; Li, X. Q.; Ren, B.; Tian, Z. Q. *J. Phys. Chem. B* **1999**, *103*, 4218.

(8) (a) Mrozek, M. F.; Weaver, M. J. *J. Am. Chem. Soc.* **2000**, *122*, 150. (b) Luo, H.; Weaver, M. J. *Langmuir* **1999**, *15*, 8743.

(9) (a) Chan, H. Y. H.; Zou, S.; Weaver, M. J. *J. Phys. Chem. B* **1999**, *103*, 11141. (b) Zou, S.; Chan, H. Y. H.; Williams, C. T.; Weaver, M. J. *Langmuir* **2000**, *16*, 754.

(10) Mrozek, M. F.; Weaver, M. J. *J. Phys. Chem. B.* **2001**, *105*, 8931.

(11) (a) Zou, S.; Williams, C. T.; Chen, E. K.-Y.; Weaver, M. J. *J. Am. Chem. Soc.* **1998**, *120*, 3811. (b) Zou, S.; Williams, C. T.; Chen, E. K.-Y.; Weaver, M. J. *J. Phys. Chem. B* **1998**, *102*, 9039 [also see erratum: Zou, S.; Williams, C. T.; Chen, E. K.-Y.; Weaver, M. J. *J. Phys. Chem. B* **1998**, *102*, 9743].

(12) (a) Gao, P.; Weaver, M. J. *J. Phys. Chem.* **1985**, *89*, 5040. (b) Gao, X.; Davies, J. P.; Weaver, M. J. *J. Phys. Chem.* **1990**, *94*, 6858.

(13) Gao, X.; Zhang, Y.; Weaver, M. J. *J. Phys. Chem.* **1992**, *96*, 4156.

(14) Gao, P.; Gosztola, D.; Leung, L.-W. H.; Weaver, M. J. *J. Electroanal. Chem.* **1987**, *233*, 211.

(15) (a) Wilke, T.; Gao, X.; Takoudis, C. G.; Weaver, M. J. *J. Catal.* **1991**, *130*, 62. (b) Gao, X.; Zhang, Y.; Weaver, M. J. *Langmuir* **1992**, *8*, 688.

(16) Gao, P.; Gosztola, D.; Leung, L. H.; Weaver, M. J. *J. Electroanal. Chem.* **1987**, *233*, 211.

(17) Leung, L. H.; Gosztola, D.; Weaver, M. J. *Langmuir* **1987**, *3*, 45.

(18) Chan, H. Y. H.; Takoudis, C. G.; Weaver, M. J. *J. Phys. Chem. B* **1999**, *103*, 357.

(19) Hartley, F. R. *The Chemistry of Palladium and Platinum*; Applied Science: London, 1973; p 462.

arrangement mimics adequately the coordinative effects upon the aromatic intramolecular bonding of interest here. Nevertheless, DFT calculations were also undertaken by using two simple metal-cluster models. The first involves a three-atom triangular cluster in which the benzonitrile aromatic ring is oriented in the same plane, and the second utilizes a five-atom single-layer (100) cluster in which the nitrile is bound to the center atom. The metal−metal distances were fixed at their bulk-phase experimental values. While satisfactory convergence was not attained with calculations for the Pt-group coordinated clusters, reliable bond-length and vibrational-frequency data were extracted from the DFT calculations for the Au_3 cluster. Representative DFT results are therefore included below for this system. (Comparable benzonitrile bond-length data were obtained for the Au_5 and Au_3 clusters, although satisfactory vibrational frequency results were not achieved for the former system.)

While clearly less appropriate than utilizing larger metal clusters, the present approach has the advantage of computational efficiency in addition to maintaining C_{2v} symmetry, so that the individual calculated harmonic vibrational modes of the coordinated molecule can readily be compared to those of the uncoordinated molecule. All calculations employed the Amsterdam Density Functional (ADF) package,[20] using the BLYP functional[21] for the generalized gradient approximation and the Vosko−Wilk−Nusair form of the local density approximation,[22] with Slater-type atomic orbital basis sets. The inner-core electrons of all atoms, except H, were kept frozen to the following orbitals: C 1s, N 1s, Au 4f, Pt 4f, and Ir 4f. All basis sets were of double-ζ quality and C, N, and H were augmented by polarization functions. The benzonitrile bond lengths and bond angles extracted from ref 23 were used as the initial input for the geometry optimization, which employed convergence criteria of 10^{-4} and 10^{-3} hartrees for the energy and gradient, respectively, in determining the calculated equilibrium geometry. Harmonic vibrational frequencies were calculated both for this equilibrium geometry and with the metal−nitrogen bond fixed instead at 2.00 Å (vide infra) using 2-point numerical differentiation, in which negative and positive bond-length displacements are used to determine the energy gradients and compute the force constants.

Results and Discussion

Vibrational Frequencies and Mode Assignments. Representative surface-enhanced Raman (SER) spectra obtained for benzonitrile on the three Group IB metals (Cu, Ag, Au) at 0 V vs SCE, adsorbed from a 20 mM solution in 0.1 M $HClO_4$, are shown in Figure 1A. Corresponding spectra obtained on the four Group VIII metals (Rh, Ir, Pd, Pt) are illustrated in Figure 1B. A detailed summary of the resulting SER band frequencies for benzonitrile adsorbed on these seven metal surfaces is given in Table 1, along with the corresponding experimental values, ν(exp), for uncoordinated (liquid) benzonitrile. The latter were also chiefly as measured in this work, supplemented by literature values (given in parentheses).[24,25] The band assignments (numbered with the Wilson notation) are also identified in Table 1 by means of an approximate mode description. While the qualitative physical nature of most of these normal modes has been described in analyses by Varsanyi,[24] the present DFT calculations also yield a complete picture of the vibrational

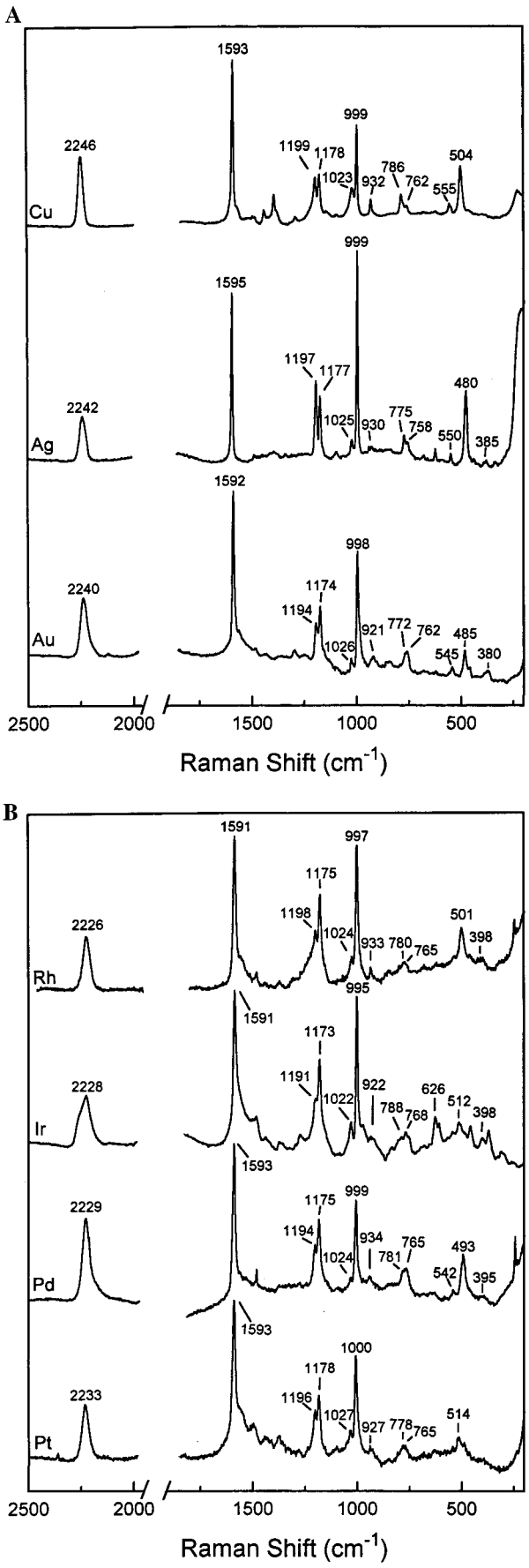

Figure 1. Surface-enhanced Raman spectra obtained for benzonitrile on (A) copper, silver, and gold and (B) rhodium, iridium, palladium, and platinum at 0 V vs SCE from 20 mM solution in 0.1 M $HClO_4$.

(20) (a) Amsterdam Density Functional Package, ADF 2000.03, Department of Theoretical Chemistry, Vrije Universiteit, Amsterdam, The Netherlands, 2000. (b) Baerends, E. J.; Ellis, D. E.; Ros, R. *Chem. Phys.* **1973**, *2*, 41. (c) teVelde, G.; Baerends, E. J. *J. Comput. Phys*. **1992**, *99*, 84.

(21) Becke, A. D. *Phys. Rev. A* **1988**, *38*, 3098. (b) Lee, C.; Yang, W.; Parr, P. G. *Phys. Rev. B* **1988**, *37*, 785.

(22) Vosko, S. H.; Wilk, L.; Nusair, M. *Can. J. Phys*. **1980**, *58*, 1200.

(23) Bak, B.; Christensen, D.; Dixon, W. B.; Hansen-Nygaard, L.; Rostrup-Anderson, J. *J. Chem. Phys*. **1962**, *37*, 2027.

(24) (a) Varsányi, G. *Vibrational Spectra of Benzene Derivatives*; Academic Press: New York, 1969. (b) Varsányi, G. *Assignments for Vibrational Spectra for 700 Benzene Derivatives*; Wiley: New York, 1974.

(25) (a) Green, J. H. S. *Spectrochim. Acta* **1961**, *17*, 607. (b) Jakobsen, R. J. *Spectrochim. Acta* **1964**, *21*, 127. (c) Green, J. H. S.; Harrison, D. J. *Spectrochim. Acta* **1976**, *32A*, 1279.

Table 1. Raman Frequencies (cm^{-1}) for Benzonitrile Adsorbed on Various Electrode Surfaces

			uncoordinated		SERS[f]						
description[a]	mode[b]	sym[c]	ν(DFT)[d]	ν(exp)[e]	Cu	Ag	Au	Pd	Pt	Rh	Ir
C−C−C in-plane bend	ν_{6a}	a_1	463	462	504	480	485	493	514	501	512
ring breathing	ν_1		763	768	786	775	772	781	778	780	788
C−C−C trigonal breathing	ν_{12}		1002	1002	999	999	998	999	1000	997	995
C−H in-plane bend	ν_{18a}		1030	1027	1023	1025	1026	1024	1027	1024	1022
C−H in-plane bend	ν_{9a}		1181	1180	1178	1177	1174	1175	1178	1175	1173
C−X stretch	ν_{7a}		1200	1194	1199	1197	1194	1194	1196	1198	1191
C−C in-plane stretch	ν_{19a}		1491	1490	1486	1488	1484	1484	1490	1484	1486
C−C in-plane Stretch	ν_{8a}		1600	1599	1593	1595	1592	1593	1593	1591	1591
C−C−C out-of-plane bend	ν_{16a}	a_2	394	(400)		385	380	395		398	398
C−H out-of-plane bend	ν_{10a}		833	(848)			850	850	850	850	835
C−C−C out-of-plane bend	ν_{16b}	b_1	546	551	555	550	545	542	542	536	544
C−H out-of-plane bend	ν_{11}		757	754	762	758	762	765	765	765	768
C−H out-of-plane bend	ν_{17b}		915	(926)	932	930	921	934	927	933	922
C−C−C in-plane bend	ν_{6b}	b_2	633	626	622	626	624	628	626	626	626
C−H in-plane bend	ν_{18b}		1169	1162							
C−H in-plane bend	ν_3		1310	(1290)	1290		1298		1280		1270
C−C in-plane stretch	ν_{14}		1337	(1336)	1392	1390	1375	1375	1375	1375	1375
C−C in-plane stretch	ν_{19b}		1445	1449	1444		1440		1440	1445	1440
CN stretch	ν_{CN}	a_1	2247	2232	2246	2242	2240	2229	2233	2226	2228
					[10]	[13]	[17]	[9]	[14]	[16]	[18]

[a] Approximate mode description, extracted chiefly from discussions in ref 24a, along with DFT analysis (see text). [b] Wilson notation for normal vibration, from ref 24. [c] Symmetry group of vibration. [d] Vibrational frequencies calculated by DFT, scaled by 0.975 (so to align with experimental values, see text). [e] Raman frequencies for liquid benzonitrile, from present measurements, except those in parentheses, which were extracted from refs 24 and 25. [f] SER frequencies for benzonitrile adsorbed at 0 V vs SCE on the metal surface indicated. The values given in brackets underneath the ν_{CN} frequency for each metal are the "Stark-tuning" slopes, $d\nu_{CN}/dE$ (cm^{-1} V^{-1}), evaluated between −0.2 and 0.4 V on the Pt metals, −0.4 and 0 V on Cu and Ag, and −0.4 and 0.4 V on Au.

$x-y-z$ motion of each atom away from equilibrium. We consider below more detailed descriptions for selected modes. The utility of DFT in this regard is highlighted by the ability of the BLYP functional to predict accurately (chiefly within 5−10 cm^{-1}) the benzonitrile mode frequencies. The computational frequencies, ν(DFT), also listed in Table 1, were adjusted slightly (with a 0.975 scaling factor) to optimize agreement with the experimental values for liquid benzonitrile, ν(exp), given alongside. Matching up the ν(exp) and ν(DFT) values, along with the vibrational mode intensities, enables complete mode assignments to be made with confidence.

We have previously analyzed in detail SER spectra for benzonitrile on gold,[12] with a similar study described more recently on palladium.[11b,26] The combined frequency−band shape−intensity analysis, the last by utilizing surface selection rules,[12b] indicates a benzonitrile orientation normal (or tilted) to the metal surface, being attached via the nitrile group. The absence of substantial aromatic−surface interactions on gold was also evident from the narrow (fwhm ∼ 10 cm^{-1}) bandwidths for most aromatic ring modes (similar to the bulk liquid).[12] The nitrile stretching (ν_{CN}) vibration, however, is substantially broadened and shifted in frequency upon adsorption, indicative of direct metal−nitrile binding (Figure 1). These spectral properties, as discussed previously for adsorption on gold[12] and palladium,[11b,26] sharply contrast those observed for another monosubstituted benzene, toluene ($C_6H_5CH_3$), on the same surfaces: the latter exhibits ring vibrations that are broadened as well as shifted significantly (by ca. 10−50 cm^{-1}). Aside from constituting direct evidence for the presence of strong metal−ring interactions for toluene, consistent with the anticipated flat surface orientation, the contrasting spectral features for benzonitrile indicate further the absence of this surface bonding mode for the latter adsorbate.

Some thermodynamic and infrared spectral evidence, however, suggests that benzonitrile binds "flat" on Au(111) electrodes at more negative potentials.[27] A similar orientation has been deduced from electron energy loss spectroscopy (EELS) for benzonitrile on Cu(111)[28] and on Au(100)[29] in UHV. (Note, however, that the "flat" orientation is apparently observed even for cyanogen at clean metal−UHV interfaces, rather than the "end-on" binding observed for −CN at metal electrodes, presumably reflecting the role of solvation and other factors.[30]) Analyses of SERS data for benzonitrile on silver sols[31] and electrodes[32] suggest either "end-on" or "face-on" orientations, with the nitrile group nonetheless providing the primary surface anchor. The original SERS report of benzonitrile adsorption on gold mentioned the appearance of low-frequency "shoulders" on the ν_{12} and ν_{18a} features at negative electrode potentials,[12] suggestive of more direct surface−ring interactions (i.e., a flat orientation) under these conditions.

However, no clear-cut evidence for such potential-induced changes in the mode of benzonitrile surface binding, or the nature of the surface−adsorbate interactions, was obtained in the present study. While some details differ, the sharp ring-mode bands along with the broadened ν_{CN} feature attest to the likely similarity of nitrile surface attachment on each metal. While the spectra shown in Figures 1A and 1B refer to 0 V vs SCE, data were also obtained between −0.3 and 0.4 V in 0.1 M $HClO_4$, and down to −0.8 V in 0.1 M $NaClO_4$ (pH 11), to examine any sensitivity to the electrode potential. Most of the vibrational band frequencies listed in Table 1 do not shift perceptibly (≤2 cm^{-1}) over the potential range −0.3 to 0.4 V, commonly assessable with 0.1 M $HClO_4$ electrolyte. There are two exceptions. As reported previously on gold,[12] the nitrile (ν_{CN}) vibration blue-shifts toward higher potentials: the

(26) The SER spectrum reported originally in ref 11b for benzonitrile adsorbed on a palladium film displayed Raman bands that were broadened artifactually by the use of a wide spectrometer band-pass. A corrected spectrum, however, is reported in the erratum to that paper.[11b]

(27) Richer, J. F.; Chen, A.; Lipkowski, J. *Electrochim. Acta* **1998**, *44*, 1037.
(28) Kordesch, M. E.; Feng, W.; Stenzel, W.; Weaver, M. J.; Conroad, H. *J. Electron Spectrosc. Related Phenom.* **1987**, *44*, 149.
(29) Solomun, T.; Christmann, D.; Baumgartel, H. *J. Phys. Chem.* **1989**, *93*, 7199.
(30) Kordesch, M. E.; Stenzel, W.; Conrad, H.; Weaver, M. J. *J. Am. Chem. Soc.* **1987**, *109*, 1878.
(31) Joo, T. H.; Kim, K.; Kim, H.; Kim, M. S. *Chem. Phys. Lett.* **1985**, *117*, 518.
(32) Holze, R. *Electroanalysis* **1993**, *5*, 497.

Table 2. Selected Vibrational Frequency Shifts (cm^{-1}) for Benzonitrile Adsorbed on Various Electrode Surfaces

				frequency shifts[b] $\Delta\nu$(exp), cm^{-1}						
description	mode	sym	liq[a]	Cu	Ag	Au	Pd	Pt	Rh	Ir
C−C−C in-plane bend	ν_{6a}	a_1	462	+42	+18	+23	+31	+52	+39	+50
ring breathing	ν_1		768	+18	+7	+4	+13	+10	+12	+20
C−C−C trigonal breathing	ν_{12}		1002	−3	−3	−4	−3	−2	−5	−7
C−H in-plane bend	ν_{18a}		1027	−3	−2	−1	−3	0	−3	−5
C−H in-plane bend	ν_{9a}		1180	−2	−3	−4	−5	−2	−5	−7
C−X stretch	ν_{7a}		1194	+5	+3	0	0	+2	+4	−3
C−C in-plane stretch	ν_{19a}		1490	−4	−2	−6	−6	0	−6	−4
C−C in-plane stretch	ν_{8a}		1599	−6	−4	−7	−6	−6	−8	−8
C−H out-of-plane bend	ν_{11}	b_1	754	+8	+4	+8	+11	+11	+11	+14
C−C−C in-plane bend	ν_{6b}	b_2	626	−4	0	−2	+2	0	0	0
CN stretch	ν_{CN}	a_1	2232	+14	+10	+8	−3	+1	−6	−4

[a] Raman frequencies measured for liquid benzonitrile (see Table 1). [b] Frequency shifts observed upon benzonitrile adsorption on the metal electrode at 0 V vs SCE (data from Table 1).

Table 3. Comparison of Vibrational Frequencies (cm^{-1}) of Bis(benzonitrile)dichloroplatinum and Benzonitrile Adsorbed on Platinum

description	mode	sym	liq[a]	$PtCl_2(BN)_2$[b]	$\Delta\nu_c$(exp)[c]	Pt SERS[d]	$\Delta\nu_a$(exp)[e]
C−C−C in-plane bend	ν_{6a}	a_1	462	555	+93	514	+52
ring breathing	ν_1		768	793	+25	778	+10
C−C−C trigonal breathing	ν_{12}		1002	999	−3	1000	−2
C−H in-plane bend	ν_{18a}		1027	1027	0	1027	0
C−H in-plane bend	ν_{9a}		1180	1179	−1	1178	−2
C−X stretch	ν_{7a}		1194	1204	+10	1196	+2
C−C in-plane stretch	ν_{19a}		1490	1490	0	1492	0
C−C in-plane stretch	ν_{8a}		1599	1594	−5	1593	−6
C−H out-of-plane bend	ν_{11}	b_1	754	763	+9	765	+11
C−C−C in-plane bend	ν_{6b}	b_2	626	624	−2	626	0
C−H in-plane bend	ν_{18b}		1162	1165	+3		
CN stretch	ν_{CN}	a_1	2232	2294	+62	2233	+1

[a] Raman frequencies for liquid benzonitrile (see Table 1). [b] Raman frequencies for solid bis(benzonitrile)dichloroplatinum. [c] Frequency shift upon Pt−benzonitrile complexation. [d] SER frequencies for benzonitrile adsorbed on Pt at 0 V vs SCE (from Table 2). [e] Frequency shift upon benzonitrile adsorption on Pt.

$d\nu_{CN}/dE$ values, between 10 and 18 cm^{-1} V^{-1}, are given in brackets underneath the corresponding ν_{CN} frequencies in Table 1. The ν_{6a} ring mode also blue-shifts (albeit only slightly) toward higher potentials, with $d\nu_{6a}/dE \approx 3-7$ cm^{-1} V^{-1}. An additional ν_{CN} band appears at lower frequencies, for example at 2100−2120 cm^{-1} on gold and 2035−2055 cm^{-1} on platinum, in the alkaline electrolyte at more negative potentials, below −0.2 V. While the band position is consistent with the occurrence of a π-bonded nitrile group,[33] and hence hinting at a "flat" adsorbate orientation, the absence of this feature when using acidic and neutral electrolytes suggests that it arises instead from cyanide or related species formed by adsorbate hydrolysis.

To facilitate examination of the metal-dependent behavior, Table 2 summarizes the frequency shifts, $\Delta\nu$(exp), observed for selected modes upon binding benzonitrile to the seven metal surfaces. These eleven modes were chosen in view of their ease of experimental identification (from band intensities, bandwidths, etc). In particular, they include modes that exhibit significant $\Delta\nu$(exp) values along with sensitivity to the metal surface. Prominent among these are the ν_{6a} band, which is seen to blue-shift substantially, by ca. 20−50 cm^{-1}, upon chemisorption, along with the ν_1 feature, which also blue-shifts noticeably, by 10−20 cm^{-1} depending on the metal. It is important to note that, although these modes were identified in our earlier studies,[11b,12] more accurate metal-dependent $\Delta\nu$(exp) values have been obtained in the present work. (Aside from the present use of higher spectrometer resolution, the necessary matching of band assignments for chemisorbed and uncoordinated benzonitrile is aided considerably by the present DFT results, vide infra.) Interestingly, these ring-mode frequency shifts are comparable to, or even larger than, those for the ν_{CN} mode, which exhibits blue-shifts on the coinage metals, and largely yields red-shifts on the Pt-group surfaces. The remaining a_1 symmetry modes display smaller (<10 cm^{-1}) and metal-insensitive $\Delta\nu$(exp) values. Of the clearly identifiable *b* symmetry modes, the ν_{11} vibration is significantly red-shifted upon adsorption, especially on the Pt-group metals, while ν_{6b} is virtually unaltered (Table 2).

A basic question is whether these mode-sensitive frequency shifts reflect the occurrence of "direct" surface−ring interactions, or rather can be accounted for in terms of an inductive effect via the nitrile substituent. It is therefore of interest to elucidate whether the frequency shifts are inherent to *surface* coordination, or if they occur also for metal−benzonitrile molecular complexes. Especially given that the majority of the present DFT calculations similarly refer to benzonitrile−metal *atom* binding, we therefore have examined Raman vibrational shifts for benzonitrile coordinated in a mononuclear Pt complex, bis(benzonitrile)dichloroplatinum [$PtCl_2(BN)_2$]. The chief Raman frequencies observed for the solid-state sample are summarized in Table 3. Listed alongside are the values for benzonitrile adsorbed on platinum at 0 V, together with the resulting frequency shifts in the complexed and adsorbed states, $\Delta\nu_c$(exp) and $\Delta\nu_a$(exp), respectively. Significantly, there are close parallels in the $\Delta\nu_c$(exp) and $\Delta\nu_a$(exp) values. Thus both coordination environments yield large blue-shifts in the ν_{6a} mode, and to a lesser extent for the ν_1 and ν_{11} modes, with comparable red-shifts in the ν_{8a} vibration. The only clear behavioral difference is seen for the ν_{CN} vibration, where the complex, but not the adsorbate, exhibits a substantial blue-shift. This difference is most simply attributable to the electropositive

(33) Nakamoto, K. *Infrared and Raman Spectra of Inorganic and Coordination Compounds*, 5th ed.; Wiley: New York, 1997; Part B, pp 113−4.

Table 4. Selected Vibrational Frequency Shifts (cm^{-1}) for Benzonitrile Bound to Metal Atoms, as Calculated by DFT

			frequency shifts[b], $\Delta\nu$(DFT), cm^{-1}						
			Ir		Pt		Au		Au_3
description	mode	ν(DFT)[a] cm^{-1}	1.80 Å	2.00 Å	1.79 Å	2.00 Å	2.28 Å	2.00 Å	2.00 Å
C−C−C in-plane bend	ν_{6a}	463	+141	+35	+136	+27	+9	+53	+46
ring breathing	ν_1	763	+66	+12	+63	+12	+2	+15	+17
C−C−C trigonal breathing	ν_{12}	1002	−5	−6	−3	−3	−1	−1	−3
C−H in-plane bend	ν_{18a}	1030	−2	−2	−2	−3	−1	0	−2
C−H in-plane bend	ν_{9a}	1181	0	−4	0	−1	+1	+1	+1
C−X stretch	ν_{7a}	1200	+32	+13	+30	+12	+2	+3	+15
C−C in-plane stretch	ν_{19a}	1491	−5	−6	−5	−5	−2	−3	−2
C−C in-plane stretch	ν_{8a}	1600	−8	−7	−6	−6	−2	−5	−2
C−H out-of-plane bend	ν_{11}	757	−8	−7	−7	−6	−5	−5	−5
C−C−C in-plane bend	ν_{6b}	633	−3	−2	−4	−4	−3	−3	−5
C−H in-plane bend	ν_{18b}	1169	−3	−1	−2	−1	+3	+3	+4
CN stretch	ν_{CN}	2247	−28	−71	+1	−41	−3	−2	+16

[a] Mode frequency for uncoordinated benzonitrile as calculated by DFT, scaled slightly (by 0.975) to match experimental values (from Table 1). [b] Frequency shifts observed upon coordination of the nitrile nitrogen to the metal atom or the cluster indicated. The left-hand column for each metal lists $\Delta\nu$(DFT) values obtained for equilibrium metal−N bond distance computed by DFT, as noted in the column header. The corresponding right-hand column for each metal gives $\Delta\nu$(DFT) values calculated for a metal−N bond distance constrained at 2.00 Å (see text).

nature of Pt(II), which should enhance the degree of nitrile−Pt donation relative to the neutral Pt atom, thereby blue-shifting the ν_{CN} frequency.

Bolstered by these findings, we next intercompare the $\Delta\nu$(exp) values with corresponding calculated frequency shifts, $\Delta\nu$(DFT), obtained by coordinating the nitrile nitrogen to metal atoms. Table 4 lists the latter values extracted for the vibrational modes in Tables 2 and 3 for three 5d metals: iridium, platinum, and gold (i.e. $5d^8$, d^9, and d^{10}). For the last metal, $\Delta\nu$(DFT) values are given also for the Au_3 cluster. (While DFT calculations were also undertaken for the other metals considered here, given the approximations involved the bonding trends are most clearly discernible within such a Periodic row.) Two $\Delta\nu$(DFT) entries are given for coordination to single metal atoms. The left-hand column refers to the metal−benzonitrile complex with the metal−N bond distances, r_{M-N}, at their *equilibrium* values (as computed by DFT), given in the column header. While the r_{M-N} values are intuitively reasonable, being longer for the d^{10} metal atom (gold) than the Pt-group adducts, the differences (about 0.5 Å) are larger than expected for bonding to the different metal *surfaces*. To accommodate this, the adjacent right-hand columns list $\Delta\nu$(DFT) values calculated for the three metals in Table 4 with r_{M-N} constrained at a common "average" value, 2.00 Å. [The $\Delta\nu$(DFT) values given for the Au_3 cluster refer only to this bond length.] The sensitivity of the $\Delta\nu$(DFT) values to r_{M-N} is clearly evident, with their magnitude increasing markedly as r_{M-N} decreases for a given metal. This complication renders the metal-dependent $\Delta\nu$(DFT) values of semiquantitative value only; however, the observed sensitivity of the frequency shifts to the vibrational mode is qualitatively unaffected by the choice of r_{M-N}.

Comparison between the corresponding $\Delta\nu$(DFT) values for a single Au atom and the Au_3 cluster in Table 4 (both for r_{M-N} = 2.00 Å) indicates a close similarity for most aromatic ring modes, although the "substituent" vibrations ν_{7a} and ν_{CN} are blue-shifted significantly for only the Au trimer. These differences are unsurprising given that ν_{7a} and especially ν_{CN} should be most closely coupled with the metal. More significantly, however, the Au monomer and trimer yield large, but closely similar, blue-shifts for the ν_{6a} and ν_1 ring modes. Overall, the above trends therefore support the semiquantitative validity of utilizing single metal atoms in the DFT calculations as a means of mimicking the perturbations of at least the aromatic ring vibrations induced upon benzonitrile chemisorption.

The comparison between the corresponding $\Delta\nu$(exp) values with these $\Delta\nu$(DFT) estimates given in Tables 2 and 4, respectively, is very informative. Most significantly, the modes displaying moderate or large positive $\Delta\nu$(exp) values are mirrored largely by significant or substantial $\Delta\nu$(DFT) values. In particular, the two modes, ν_{6a} and ν_1, which exhibit the largest $\Delta\nu$(exp) values yield similarly pronounced $\Delta\nu$(DFT) estimates. Of the remaining ring modes, only the ν_{7a} vibration shows large $\Delta\nu$(DFT) values for the Pt-group metals, but not for gold (Table 4). This finding is in harmony with the behavior of the Pt−benzonitrile complex (Table 3) but not the metal surfaces, reflecting bonding differences in these coordination environments. However, the small ($\lesssim$10 cm^{-1}) $|\Delta\nu$(DFT)| values seen for the remaining ring modes largely match the experimental behavior, with the exception of the ν_{11} vibration.

Relation to Chemisorption-Induced Electron Polarization and Bond-Length Changes. The observation of a broad concordance between the mode-dependent $\Delta\nu$(exp) and $\Delta\nu$(DFT) behavior gives us sufficient confidence in the reliability of the DFT calculations for mimicking the effects of metal surface, as well as metal atom, coordination to utilize this approach to interpret the experimental wavenumber shifts in terms of chemisorption-induced electronic polarization and intramolecular bond-length changes. Table 5 lists the electronic charges, q, residing on each atom of uncoordinated benzonitrile, as estimated by DFT with the Mulliken method,[34] along with the charge changes (Δq) seen upon metal coordination for the same r_{M-N} distances as in Table 4. (The atom numbering system used in Table 5 is clarified in the structure shown in Figure 2.) While estimating such "absolute" atomic charges suffers from some arbitrariness, at least the *changes* in electron density upon coordination, of primary interest here, should approximately be represented by the Δq values. Summarized in Table 6 are equilibrium bond distances, r, calculated by DFT for free benzonitrile and the changes, Δr, induced upon coordination to Ir, Pt, and Au atoms and to Au_3, as before. The uncoordinated r values are uniformly close to those estimated from microwave spectra for gaseous benzonitrile.[23]

Inspection of Table 5 shows that, perhaps not surprisingly, the largest coordination-induced electron-density changes occur in the nitrile substituent atoms, with the nitrogen gaining and the C7 carbon losing substantial (ca. 0.2 e^-) charge. These effects can be rationalized in terms of metal−nitrile π back-

(34) Mulliken, R. S. *J. Chem. Phys.* **1962**, *36*, 3428.

Table 5. Coordination-Induced Changes in Mulliken Charges on Benzonitrile Atoms As Calculated by DFT

		change in atomic charge,[c] Δq						
		Ir		Pt		Au		Au_3
atom[a]	uncoord. charge,[b] q	1.80 Å	2.00 Å	1.79 Å	2.00 Å	2.28 Å	2.00 Å	2.00 Å
C1	−0.143	−0.012	−0.008	−0.011	−0.007	−0.006	−0.010	−0.012
C2,6	0.088	−0.023	−0.017	−0.019	−0.014	−0.004	−0.008	−0.003
C3,5	0.042	−0.001	0.000	−0.001	0.000	+0.002	+0.002	+0.004
C4	0.044	−0.010	−0.007	−0.008	−0.006	+0.002	+0.001	+0.003
C7	0.260	+0.189	+0.216	+0.208	+0.220	+0.236	+0.258	+0.275
N	−0.426	−0.230	−0.154	−0.207	−0.140	−0.091	−0.181	−0.220
H2,6	0.030	−0.011	−0.005	−0.008	−0.004	+0.002	0.000	+0.002
H3,5	−0.019	−0.004	−0.002	−0.003	−0.001	+0.004	+0.005	+0.007
H4	−0.018	−0.006	−0.003	−0.004	−0.002	+0.005	+0.005	+0.009
M	0	+0.147	+0.003	+0.084	−0.027	−0.157	−0.071	−0.075

[a] Benzonitrile carbon and hydrogen atoms are numbered (as conventional) as shown in Figure 2. [b] Mulliken atomic charges[34] (in electron units) as estimated from the present DFT analysis for uncoordinated benzonitrile. [c] Change in Mulliken atomic charge, Δq, upon metal−benzonitrile coordination, with rM-N values indicated in column header, such that a negative Δq indicates a gain of e^- charge and a positive Δq represents a loss of e^- charge.

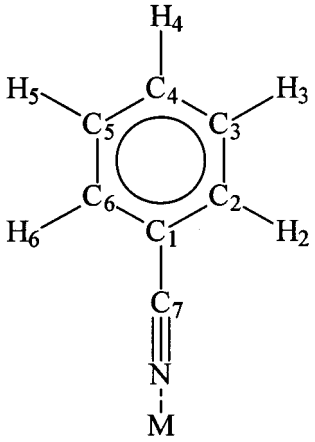

Figure 2. Structure of coordinated benzonitrile, with the atom numbering system as used in Tables 5 and 6.

donation, yielding charge residing primarily on the more electronegative N atom, together with charge induction from C7 to N produced by metal−nitrile σ donation. However, the C1 carbon (i.e. that bonded to the nitrile) along with the C2 atom experience significant increases in electron density via conjugative effects, with C4 (the para position) also gaining charge upon coordination to Pt and Ir, but not Au. This difference in bonding between the Pt-group and coinage metals is also evident in the loss and gain in their electronic charge, respectively, seen upon coordination, undoubtedly reflecting the greater π back-donating ability of the former. Indeed, this factor is probably also responsible for the ν_{CN} red-shifts, predicted by DFT upon Pt-group coordination, and the ν_{CN} blue-shifts obtained for Au_3 binding (Table 4), in qualitative accordance with the experimental metal-dependent ν_{CN} behavior (Table 2) (see also below). Significantly, closely comparable Δq values were obtained for coordination to not only the Au atom and Au_3 (Table 5) but also to the Au_5 cluster (not shown). This concordance further supports the validity of the single metal-atom DFT results for the present purposes.

Further DFT-based insight regarding coordination-induced perturbations in benzonitrile bonding is provided by the Δr values in Table 6. Nitrile coordination to Pt and Ir, but not to Au (or Au_3), is seen to significantly elongate the C−N bond (Table 6). Given the close relationship between bond vibrational frequencies and equilibrium bond lengths, commonly known as "Badger's rule",[35] the observed negative $\Delta\nu_{CN}$ values (i.e., red-shifts) observed on the Pt-group metals (Tables 2 and 3) are to be expected. Interestingly, however, the C1−C7 bond is seen to be *compressed* upon coordination, especially to Pt and Ir (Table 6). While the $|\Delta r|$ values within the aromatic moiety are relatively small, reflecting the minor changes in electron density, a net ring expansion upon Pt-group metal coordination is evident via changes in the C1−C2 and (to a lesser extent) the C3−C4 bonds. These effects are consistent with the corresponding increases in electron density at the C1 and C4 positions, indicating the occurrence of antibonding electron repulsion.

Armed with the structural information in Tables 5 and 6, it is of particular interest to examine the motion of specific carbon atoms in the various benzonitrile "ring-centered" modes to link the experimental coordination-induced vibrational behavior with the manner and degree of electron polarization and bond-length changes. (Note that, unlike the ν_{CN} mode which is largely decoupled from other vibrations due to the high C−N force constant, some "ring" modes will involve substantial vibrational coupling between the aromatic ring and substituent motions.) The ADF-DFT output provides detailed information regarding the various atomic displacements, the salient aspects of which are now summarized for the vibrational modes of particular interest here. Significantly, both the ν_{6a} ("in-plane bend") and ν_1 ("ring breathing") modes involve substantial C1−C7−N stretching motions, especially the C1−C7 bond, with the ring and substituent distortions being in-phase and out-of-phase, respectively. The third coordination-sensitive vibration according to DFT (and seen experimentally for the Pt−benzonitrile complex), the ν_{7a} ("C−X stretching") mode, also involves C1−C7 stretching coupled with ring motion. In contrast, the ν_{12} ("C−C−C trigonal breathing") and ν_{18a} ("C−H in-plane bending") modes feature ring distortion *without* any C1−C7−N stretching motion. The same situation also applies to the ν_{9a} ("C−H in-plane bend") mode. The sole identifiable b_1 symmetry mode, ν_{11}, also involves some degree of C1−C7−N stretching coupled with bending motion. Although this mode yields small negative $\Delta\nu$(DFT) values (Table 4), larger positive $\Delta\nu$(exp) values are obtained in both the Pt-complex and chemisorbed environments (Tables 2,3).

Consequently, then, the presence of moderate or substantial vibrational frequency shifts for certain "ring modes" upon nitrile-induced benzonitrile complexation or chemisorption apparently emanates from an involvement of C1−C7−N stretching in the coupled motion, given the above finding of substantial coordination-induced electron density and bond-length alterations in

(35) Nakamoto, K. *Infrared and Raman Spectra of Inorganic and Coordination Compounds*, 5th ed.; Wiley: New York, 1997; Part A, p 15.

Table 6. Coordination-Induced Changes in Benzonitrile Bond Lengths, Δr (Å), as Calculated by DFT

		bond length changes,[c] Δr, Å						
	uncoord.[b]	Ir		Pt		Au		Au_3
bond[a]	*r*, Å	1.80 Å	2.00 Å	1.79 Å	2.00 Å	2.28 Å	2.00 Å	2.00 Å
C1−C2	1.388	+0.006	+0.006	+0.005	+0.004	+0.001	+0.002	+0.002
C2−C3	1.375	−0.002	−0.001	−0.002	−0.002	−0.001	−0.001	−0.002
C3−C4	1.380	+0.001	+0.001	+0.001	+0.001	0	0	0
C1−C7	1.411	−0.017	−0.015	−0.017	−0.015	−0.004	−0.007	−0.013
C7−N	1.154	+0.010	+0.005	+0.006	+0.002	−0.002	+0.001	−0.003

[a] The bond numbering system is shown in Figure 2. [b] The equilibrium bond distance in uncoordinated benzonitrile, as estimated by DFT. [c] Change in equilibrium bond distances upon coordination to the metal atom indicated, as estimated by DFT, such that a negative Δr indicates a shortening and a positive Δr represents a lengthening of the bond.

the C1−C7−N moiety (Tables 5 and 6). Most significantly, Badger's rule can readily account for the marked coordination-induced *blue-shifts*, i.e., positive $\Delta\nu$(exp) [and $\Delta\nu$(DFT)] values, observed especially for the ν_{6a} and ν_1 vibrations, given that the Cl−C7 bond *compresses* significantly upon Pt-group coordination (Table 6). Even though the ν_{6a} and ν_1 vibrations involve coupled ring−C1−C7−N distortion, and the nitrile ν_{CN} ("isolated C−N motion") exhibits a red-shift (for Pt and Ir) along with C7−N bond elongation (vide supra), the dominance of the C1−C7 motion in these coupled modes undoubtedly leads to the net observed blue-shifts. Since small or negligible $\Delta\nu$(exp), as well as $\Delta\nu$(DFT), values are obtained for modes featuring purely aromatic ring motion, one may conclude that the minor changes in electron density obtained for the C1, C2, C6, and C4 atoms do not contribute primarily to the observed frequency shifts, at least not for the ν_{6a}, ν_{11}, and ν_{7a} modes. Nevertheless, the small (<10 cm^{-1}) yet detectable red-shifts, i.e., negative $\Delta\nu$(exp) as well as $\Delta\nu$(DFT) values, observed for the ν_{12}, ν_{18a}, and ν_{19a} vibrations (Tables 2−4) can readily be linked (via Badger's rule) with the net ring expansion associated with the C1−C2 and C3−C4 bonds (Table 6), attributed to the increases in antibonding electron density on the C1, C2, and C4 atoms (Table 5).

While this analysis is largely descriptive, it evidently provides a self-consistent rationale for the notable sensitivity of the metal coordination-induced frequency shifts, in sign as well as magnitude, to the coupled nature of normal-mode vibrations on the basis of localized bonding perturbations.

Metal-Dependent Chemisorbate Bonding. As noted at the onset, a central theme in this study concerns understanding the manner in which the metal surface−adsorbate binding depends on the electrode material. Even though we have already alluded to this issue in the foregoing discussion, it is appropriate here also to summarize some overall metal-dependent trends as extracted from the present combined SERS-DFT approach. In general, nitrile coordination to metals is expected to involve both ligand−metal σ donation and π back-donation. Similarly to metal carbonyls, since the latter bonding mode involves an antibonding nitrile orbital its occurrence is expected to induce ν_{CN} red-shifts.[33] Examination of the metal-dependent SERS ν_{CN} behavior (Tables 1 and 2) shows that the ν_{CN} frequencies red-shift in the sequence Cu < Ag < Au $\lesssim$ Pt < Pd $\sim$ Rh $\sim$ Ir. While the experimental ν_{CN} differences are small, these trends therefore suggest that the extent of metal−nitrile back-donation increases from right to left in the Periodic series, i.e., in the sequence $d^{10} < d^9 \lesssim d^8$. This observation [also mimicked by DFT (Table 4)] is consistent with theoretical expectations,[36,37] including those based on recent DFT calculations,[36] indicating that the metal d-band center moves up in energy as one progresses from right to left along a Periodic row, thereby encouraging back-donation. Similar trends are also seen from recent DFT calculations for CO chemisorbed on Pt-group (111) surfaces,[38] although the experimental metal-dependent variations in CO stretching frequencies are complicated by differences in preferred bonding-site geometries and other bonding factors. Given the limitations of the present DFT calculations for predicting the $\Delta\nu_{CN}$ values, alluded to above, a reliable general analysis of these metal-dependent trends would clearly require the use of larger cluster (or even slab) surface models; this is beyond the scope of the present work.

Of course, however, the major virtue of the present coupled SERS-DFT results, especially compared to IRAS data, is in our ability to discern metal-dependent trends in vibrational frequencies for numerous other intramolecular adsorbate modes. Of particular significance in this regard are the "aromatic-ring" modes, most prominently ν_{6a} and ν_1, that involve substantial coupled C1−C7−N motion, especially the C1−C7 bond. The coordination-induced blue-shifts in these modes, driven by C1−C7 bond compression as noted above, exhibit similar trends along a Periodic row as for the ν_{CN} red-shifts, increasing in the order Au < Pt < Ir and Ag < Pd $\lesssim$ Rh (Table 2). This sequence, $d^{10} < d^9 < d^8$, is again captured by the corresponding DFT-based frequency shifts (Table 4). The corresponding DFT bond-length data (Table 6) show that this sequence is mirrored most notably by greater C1−C7 bond compression. The nature of these metal-dependent trends suggests strongly that the coordination-sensitive ring-mode blue-shifts are also triggered chiefly by metal−adsorbate back-donation, acting now to *strengthen* the C1−C7 bond.

It remains to consider the metal-dependent nature of the small, yet measurable, coordination-induced red-shifts of ring modes, such as ν_{12}, ν_{18a}, ν_{9a}, ν_{19a}, and ν_{8a} (Table 2), that do not involve significant contributions from C1−C7−N motion. These trends in SERS frequencies, also mirrored largely by the DFT calculations (Table 4), exhibit metal-dependent red-shifts, again in the sequence $d^{10} < d^9 < d^8$. Table 6 shows that these "pure ring-mode" red-shifts correlate primarily with increases in the C1−C2 bond distances, with smaller changes in C2−C3 and C3−C4 bonds. Examination of the corresponding Mulliken charges in Table 5 suggests that these mode frequency and bond-distance changes arise from alterations in the antibonding ring electron density in the sequence $d^{10} < d^9 < d^8$.

Consequently, then, these ring-mode red-shifts, along with the larger blue-shifts seen for coupled ring-substituent motion and the ν_{CN} mode red-shifts, each exhibit metal-dependent trends that are consistent with metal−adsorbate back-donation increas-

(36) Hammer, B.; Nørskov, J. K. *Adv. Catal.* **2000**, *45*, 71.
(37) (a) Sung, S.-S.; Hoffmann, R. *J. Am. Chem. Soc.* **1985**, *107*, 578. (b) Shustorovich, E.; Baetzold, R. C.; Muetterties, E. L. *J. Phys. Chem.* **1983**, *87*, 1100.
(38) (a) Koper, M. T. M.; van Santen, R. A.; Wasileski, S. A.; Weaver, M. J. *J. Chem. Phys.* **2000**, *113*, 4392. (b) Wasileski, S. A.; Koper, M. T. M.; Weaver, M. J. *J. Phys. Chem. B* **2001**, *105*, 3518.

ing from right to left along a given Periodic row (i.e. $d^{10} < d^9 < d^8$). The behavioral differences between the 4d and 5d series are more subtle, although red-shifts for the "pure ring-mode" vibrations as well as the blue-shifts for the "coupled ring-substituent" modes appear to be more pronounced for the 5d than for the corresponding 4d metals (Table 2).

Concluding Remarks

The present findings are considered to provide a clear illustration of the utility of our "overlayer SERS" strategy for exploring metal-dependent bonding of complex organic adsorbates in electrochemical environments. The excellent (≤ 1 cm^{-1}) wavenumber resolution of SERS, combined with its ability to detect a large fraction of the chemisorbate normal modes, enables uniquely detailed vibrational information to be extracted, even at metal−solution interfaces. The value of DFT for aiding band assignments, as well as the fundamental interpretation of the chemisorbate vibrational properties in terms of surface bonding, is also clearly evident. While the present DFT calculations, mimicking surface coordination by using a single metal atom or small metal cluster, are somewhat crude, more realistic surface models employing finite clusters or slabs can in principle be utilized, albeit at the (perhaps substantial!) cost of computational efficiency.[36,39] The effect of the variable surface potential in electrochemical systems can also be monitored by applying external electrostatic fields.[38,40] Such field-dependent vibrational DFT calculations have so far focused on small chemisorbates such as CO, similar to the emphasis placed in modeling metal−UHV interfaces by DFT. Nevertheless, there are clearly considerable opportunities for gaining a deeper understanding of metal−chemisorbate bonding for molecularly more complex adsorbates, such as the present example, by combining vibrational spectroscopy with DFT model calculations. Further studies along these general lines for organic as well as inorganic adsorbates at electrochemical interfaces, emphasizing SERS and/or IRAS measurements combined with DFT, are being pursued in our laboratory.

Acknowledgment. This work is supported by the National Science Foundation (Analytical and Surface Chemistry Program) and by the Petroleum Research Fund, administered by the American Chemical Society.

JA010049K

(39) For example: van Santen, R. A.; Neurock, M. *Catal. Rev.-Sci. Eng.* **1995**, *37*, 557.

(40) For example: (a) Head-Gordon, M.; Tulley, J. C. *Chem. Phys.* **1993**, *175*, 37. (b) Illas, F.; Mele, F.; Currulla, D.; Clotet, A.; Ricart, J. M. *Electrochim. Acta* **1998**, *44*, 1213.